Draft version May 4, 2025
Typeset using LaTeX **twocolumn** style in AASTeX7

The Sunyaev Zel'dovich Effect in the Context of Galaxy Formation and Evolution

Justin Bak[1]
ASTRO 6590: Galaxies and the Universe

[1] *Cornell University*

ABSTRACT

This research paper is intended to accomplish four goals: 1.) understand the physical processes that govern both the thermal Sunyaev-Zel'dovich effect (tSz) and kinetic Sunyaev-Zel'dovich effect (kSz) 2.) contrast different cosmological methods that have been used to study the Sunyaev Zel'dovich effect 3.) discuss models that are used to effectively model feedback from supernovae and active galactic nuclei (AGN) 4.) understand the implications of the Sunyaev-Zel'dovich effect on circumgalactic medium (CGM) and intracluster medium (ICM)

Keywords: Galaxies (573) — Cosmology (343) — High Energy astrophysics (739)

1. INTRODUCTION

The Cosmic Microwave Background (CMB) is one of the best indicators of our early universe. It is composed of uniform microwave radiations, with small anisotropies on the order of 1 part in 100,000. These fluctuations contain the seeds of all large-scale galaxy structures, including clusters, and originate from inverse Compton scattering. The presence of these holes in the cosmic microwave background is indicative of a larger phenomenon: the Sunyaev Zel'dovich Effect.

2. PHYSICAL PROPERTIES THAT GOVERN THE SUNYAEV-ZEL'DOVICH EFFECT

The Sunyaev-Zel'dovich Effect can be split into two separate classifications: the thermal Sunyaev-Zel'dovich Effect (tSz) and the kinetic Sunyaev-Zel'dovich Effect (kSz). To understand the former, we must first examine inverse Compton scattering. Compton scattering can be defined by:

$$\lambda' - \lambda = \frac{h}{m_e c}(1 - \cos\theta)$$

In Compton scattering, a high-energy photon hits an electron, which causes the electron to gain some energy from the photon. As a result, the electron recoils and the photon is scattered away with lower energy R. A. Sunyaev & Y. B. Zel'dovich (1972). As seen from the equation, the change in wavelength depends only on the scattering angle, and not the original energy of the photon. Conversely, inverse Compton scattering occurs when a high-energy electron transfers energy to a low-energy photon, boosting the energy of the photon. The photon simultaneously absorbs some of the electron's energy and scatters with a much higher frequency than its original state.

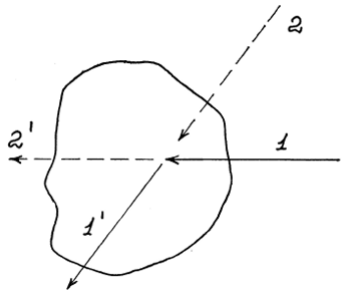

Figure 1. Inverse Compton Scattering R. A. Sunyaev & Y. B. Zel'dovich (1972)

The scattering of CMB photons occasionally pass through galaxy clusters, which contain hot, ionized gas (on the order of 10^7–10^8 K). In this case, some of the photons gain energy, which creates a dip in intensity at low frequencies and a bump at high frequencies J. E. Carlstrom et al. (2002). Thus, a non-blackbody distortion is created in the CMB. This phenomenon is known as the thermal Sunyaev-Zel'dovich Effect (tSz) R. A. Sunyaev & Y. B. Zel'dovich (1980). It is important

Email: jb2757@cornell.edu

to note that this distortion is independent of redshift, making this effect extremely useful for studying distant galaxy clusters. As previously discussed, the Sunyaev-Zel'dovich Effect indicates a fluctuation in the CMB. In the case of the thermal Sunyaev-Zel'dovich Effect, this fluctuation can be described as:

$$\frac{\Delta T_{\rm tSZ}}{T_{\rm CMB}} = f(\nu)\, y$$

where the frequency dependence is given by:

$$f(\nu) = x\, \coth\left(\frac{x}{2}\right) - 4, \quad \text{where} \quad x = \frac{h\nu}{k_B T_{\rm CMB}}$$

It is important to define y, which quantifies how much energy is transferred from hot electrons to photons as the photons pass through a plasma of high-energy electrons, such as the hot gas in a galaxy cluster. This is known as the Compton y-parameter:

$$y(\theta) = \frac{\sigma_T}{m_e c^2} \int_{\rm los} P_e \left(\sqrt{l^2 + d_A(z)^2 |\theta|^2}\right) dl$$

There is another important component of the Sunyaev-Zel'dovich Effect that preserves the black-body shape of the CMB. In the kinetic Sunyaev-Zel'dovich Effect (kSz), CMB photons scatter off electrons that are moving with a bulk velocity relative to the cosmic rest frame. In other words, the kinetic Sunyaev Zel'dovich effect (kSz) is a Doppler shift of the CMB photons, in which the frequency of a wave as observed by someone who is moving relative to the source of the wave. The kSZ temperature fluctuations are given by:

$$\frac{\Delta T_{\rm kSZ}}{T_{\rm CMB}} = \frac{\sigma_T}{c} \int_{\rm los} e^{-\tau} n_e\, v_p\, dl,$$

where n_e is the electron number density, v_p is the peculiar velocity, and τ is the optical depth to Thomson scattering along the line of sight, defined as:

$$\tau(\theta) = \sigma_T \int_{\rm los} n_e \left(\sqrt{l^2 + d_A(z)^2 |\theta|^2}\right) dl.$$

This relationship is sometimes simplified to:

$$\frac{\Delta T_{\rm kSZ}}{T_{\rm CMB}} = \tau_{\rm gal} \left(\frac{v_r}{c}\right),$$

where $\tau_{\rm gal}$ refers to the optical depth of the galaxy group considered, and $v_r = 1.06 \times 10^{-3} c$ is the RMS of the peculiar velocities, projected along the line of sight, where the magnitude adopted is for the median redshift of the CMASS sample, $z = 0.55$, in the linear approximationJ. E. Carlstrom et al. (2002).

The fluctuations from the Sunyaev Zel'dovich effect (SZE) have been commonly described through the relationship below:

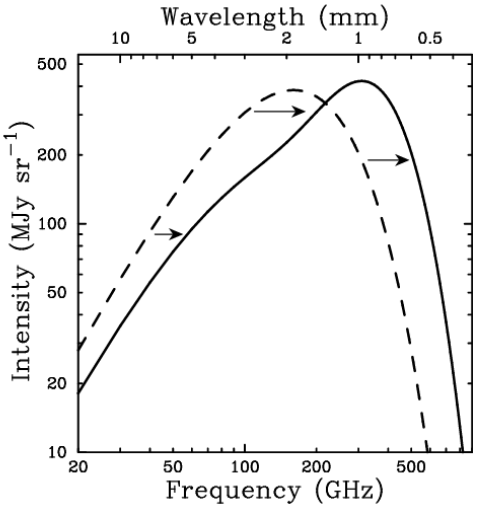

Figure 2. The Cosmic Microwave Background (CMB) spectrum, undistorted (dashed line) and distorted by the Sunyaev-Zel'dovich effect (SZE) (solid line) J. E. Carlstrom et al. (2002)

As seen in the figure, the unperturbed curve shifts to the right as a result of the SZE, indicating a peak of intensity at a higher observation frequency.

3. COSMOLOGY WITHIN THE CONTEXT OF THE SUNYAEV ZEL'DOVICH EFFECT

At this point, you may be wondering– so what? Why does the Sunyaev Zel'dovich effect (SZE) matter in the realm of astronomy? As it turns out, the SZE is able to trace both the density and pressure profiles of galaxy clusters. These profiles serve as very helpful indications of how baryons are distributed through galaxy formation and evolution. Understanding this behavior gives us clues for the 'missing baryon problem' and can even be used to estimate the Hubble parameter.

Fortunately, the SZ signal depends only on the integrated electron pressure, not on distance. This means the SZ effect can be used to detect distant galaxy structures, unlike X-ray surveys. The tSz effect can detect hot electrons even in low-density regions like the the intracluster medium (ICM). The kSZ signal is linearly proportional to electron number density, and the integrated kSZ scales linearly with halo mass. This means kSz can reveal bulk motions of baryons, even when they're too cool or diffuse for X-ray detection. Conversely, the tSZ signal is proportional to the integrated pressure ($P_e \propto n_e T_e$). In more massive halos the electron tem-

perature is higher. Therefore, the tSz signal scales as a higher power of halo mass ($\propto M^{5/3}$). Most of the contribution from the tSz signal will be from the most massive object in a given sample. In essence, both the tSz and kSz must be used in tandem to effectively measure the thermodynamic properties of a given sample of galaxies/clusters.

In this paper, we will examine data from the Baryon Oscillation Spectroscopic Survey (BOSS), the Atacama Cosmology Telescope (ACT) and Planck. In the figure below, BOSS galaxies are coded based on their line-of-sight (LOS) velocity, with blue points coming towards us, and red points traveling away from us. Grey points are neutral. The CMB map beyond the BOSS data is compiled through both tSz and kSz effects, where the tSz effect is obtained by stacking the CMB map over the position of the BOSS galaxies at their respective points. The kSz effect is estimated by weighting the LOS velocity. In this particular figure, the radial direction corresponds to comoving distances bewteen galaxies. Axes indicate comoving radial distance and redshift, respectively.

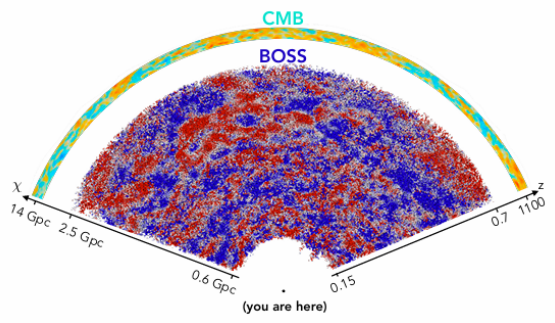

Figure 3. CMB and BOSS Data E. Schaan et al. (2021)

The figure shows a snapshot of some of the earliest known moments in the Universe, compiled with the three dimensional examination of galaxy velocities by BOSS. In combining the photons emitted by the CMB with the structure from BOSS, we can trace how tiny fluctuations in the early universe evolved into the complex cosmic web of galaxies and clusters we observe today.

3.1. *Differences in Surveys*

The first survey of import in this paper is that of Planck, a space-based satellite observatory operated by the European Space Agency which observed the entire sky in multiple frequency bands. This survey was able to detect the thermal SZ (tSZ) effect by observing distortions in the cosmic microwave background (CMB) caused by hot gas in galaxy clusters. Although its resolution was relatively coarse, Planck's full-sky coverage made it ideal for building the largest catalog of SZ-detected clusters and studying cosmological parameters linked to cluster abundance and distribution.

Although it can observe a much smaller portion of the sky, the Atacama Cosmology Telescope (ACT), located in Chile, complements Planck with much higher angular resolution. ACT is optimized to detect both the thermal and kinetic SZ (kSZ) effects with greater precision, allowing it to resolve individual clusters and probe subtler distortions. Importantly, ACT has been instrumental in detecting the kSZ signal from moving ionized gas, including diffuse baryons in cosmic filaments, by stacking data across many structures.

Finally, BOSS (Baryon Oscillation Spectroscopic Survey) is not an SZ detector itself, but plays a crucial supporting role. As part of the Sloan Digital Sky Survey (SDSS), BOSS maps the positions and redshifts of millions of galaxies, providing the large-scale structure and velocity information necessary to interpret SZ signals. Its galaxy catalogs have been used in conjunction with ACT's CMB maps to reconstruct velocity fields and detect the kSZ signal statistically, helping locate missing baryons that don't emit light directly.

3.2. *Single Disk Observations*

The first measurements of the SZ effect were made with single dish radio telescopes at centimeter wavelengths. Single dish telescopes measure the SZ effect using differential methods, which require switching the beam position to distinguish the faint SZ signal from instrumental and atmospheric systematics. Techniques like Dicke switching and cutting mirrors are used to remove offsets and temperature drifts, significantly reducing efficiency. Early SZE detections using single dish radio telescopes were often inconsistent due to systematics. Progress was made by Birkinshaw and others using the OVRO 40m and later the 5m telescope at 32 GHz. Instruments like SEST, IRAM, and Nobeyama followed, utilizing bolometric detectors and chopping techniques at higher frequencies (21–150 GHz) to study SZE in clusters more reliably. Although single disk observations can model the SZ effect on considerable accuracies, the need for differential methods in observation highlights the requirement a more practical method.

3.3. *Interferometric Observations*

A new competitor enters the race to accurately model the SZ effect– interferometric observation. Unlike single-disk observation, interferometric observation utilizes spatial filtering, which leads to stable, high quality imaging. Interferometry works by compiling information

from multiple telescopes. In general, all interferometric arrays can be modeled as a collection of $n(n-1)/2$ two element interferometers. In general, interferometry turns a series of telescopes into a 'synthetic aperture': a virtual telescope as large as the distance between the telescopes. However, unlike a camera that directly forms an image, an interferometer measures components of the Fourier transform of luminosity.

For each pair of telescopes, an interferometer effectively scales the brightness of the sky by a cosine factor, then integrates this product and outputs the time average amplitude. In practice, these signals are split and two correlations are performed. One of these correlations performs a 90 degree relative phase shift so that the output of the interferometer is the complex Fourier transform of the sky brightness. This is known as the visibility. In interferometry, the vector between two telescopes is known as the baseline, which determines the angular scale at which the pair is sensitive to. Short baselines are sensitive to large-scale galaxy structures, while longer baselines are sensitive to smaller structures. When a pair of telescopes receives a signal, it samples the Fourier transform of the sky's brightness at a specific spatial frequency (u, v), determined by:

$$u = \frac{B_x}{\lambda}, \quad v = \frac{B_y}{\lambda}$$

As mentioned previously, the visibility is determined from the integration of both components:

$$V(u,v) = \iint I(l,m)\, e^{-2\pi i(ul+vm)}\, dl\, dm$$

This expression is a two-dimensional Fourier transform of the sky intensity $I(l, m)$, where l and m are angular coordinates on the sky. Unlike single disk observations, interferometers reject large-scale background noise as they only respond to specific angular scales. Furthermore, the long baseline components of interferometry can resolve smaller structures, like subclusters, which would be impossible in a single disk observation. Ultimately, the natural proclivity for interferometry to reject noise is a highly desirable factor when considering observation of the SZ effect. The OVRO and BIMA SZE imaging project use 30 GHz (1 cm) low-noise receivers mounted on the OVRO and BIMA mm-wave arrays in California. A sample of their images can be seen below:

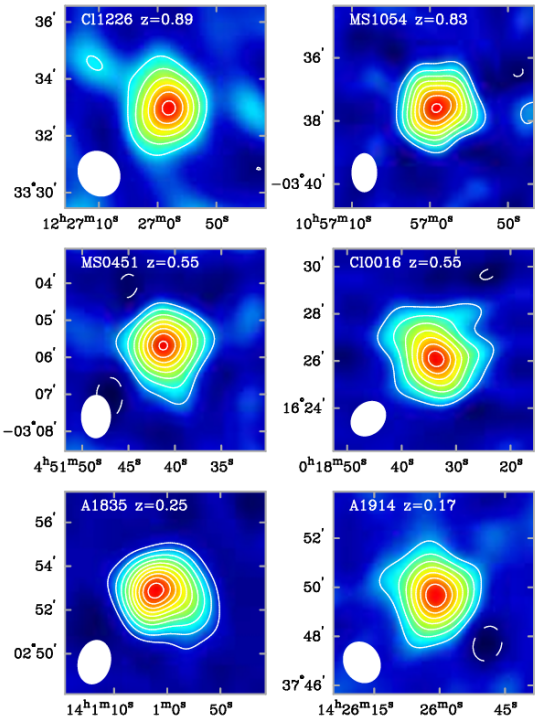

Figure 4. Deconvolved interferometric SZE images for a sample of galaxy clusters over a large redshift range ($0.17 \leq z \leq 0.89$). The contours are multiples of 2σ and negative contours are shown as solid lines. The noise level σ ranges from 25 μK to 70 μK for the clusters shown. Radio point sources were removed from a large fraction of the images shown J. E. Carlstrom et al. (2002)

As seen in the figure, the interferometer was able to separate the point source emission from the SZE by using high resolution data obtained with long baselines. The strength of the SZE signals are similar despite the high range of redshift, highlighting the independence of the Sunyaev Zel'dovich effect on redshift.

4. A DISCUSSION ON SUPERNOVAE AND ACTIVE GALACTIC NUCLEI (AGN) FEEDBACK

In this section, we aim to discuss the discrepancies of cosmological models of SZE given a few feedback optimization models. These models originate from "The Atacama Cosmology Telescope: Modeling the Gas Thermodynamics in BOSS CMASS galaxies from Kinematic and Thermal Sunyaev-Zel'dovich Measurements", in which constraints are placed on the gas thermodynamics of constant stellar mass galxies in the Baryon Oscillation Spectroscopic Survey (BOSS) using new measurements of kSZ and tSZ signals. The three models used in the paper are: the OBB Model, GNFW pressure model, and GNFW density model.

4.1. *OBB Model*

The OBB Model is based upon assuming the gas of a given radius has an initial energy per unit mass equivalent to that of its dark matter halo. To achieve this, it is assumed that the dark matter follows a spherically symmetric Navarro-Frenk-White (NFW) profile, characterized by a density normalization ρ_0 and a scale radius r_s:

$$\rho_{\rm DM}(x) = \frac{\rho_0}{x(1+x)^2},$$

where $x \equiv r/r_s$. The scale radius is related to the halo mass through the concentration parameter $c_{\rm NFW}$, with $r_s = R_{200}/c_{\rm NFW}$. In previous papers, it has been established that the power-law relation for halo masses in the range of consideration ($10^{11} - 10^{15} h^{-1} M_\odot$ at $0 < z < 2$) is:

$$c_{\rm NFW} = 5.71 \times (1+z)^{-0.47} \times \left(\frac{M}{2\times 10^{12} M_\odot}\right)^{-0.084}.$$

Furthermore, it is assumed that the initial gas mass is a fraction of the total halo mass, characterized by the baryon fraction. Using this assumption, we can use the virial theorem to get the gas energy and surface pressure in terms of the dark matter halo parameters. Finally, the model assumes that both pressure and density follow a polytropic distribution characterized by a central pressure and density:

$$\rho_{\rm gas}(r) = \rho_0 \theta(r)^{\frac{1}{\Gamma-1}}$$

$$P_{\rm tot}(r) = P_0 \theta(r)^{\frac{1}{\Gamma-1}+1},$$

where Γ is the polytropic index and $\theta(r)$ is the polytropic variable, defined as:

$$\theta(r) = 1 + \frac{\Gamma-1}{\Gamma}\frac{\rho_0}{P_0}\left(\Phi_0 - \Phi(r)\right)$$

To find the gas distribution, the conservation of energy law is used in tamdem with the boundary condition: the final gas energy E_f will be equal to the initial energy E_i plus the energy injected by feedback processes, $\epsilon M_\star c^2$, where ϵ is a dimensionless parameter quantifying the efficiency of the feedback and $M_\star$ is the stellar mass, plus the energy ΔE_p due to expansion or contraction of the halo boundaries:

$$E_f = E_i + \epsilon M_\star c^2 + \Delta E_p,$$

Ultimately, the OBB model is used to constrain a non-thermal pressure profile, $\alpha_{\rm Nth}$, and the energy injected in the gas by feedback, ϵ. Battaglia et al found that for massive clusters ($M_{\rm tot} = 10^{14} h^{-1} M_\odot$), simulations with a polytropic index $\Gamma = 1.2$, a fraction of the baryonic mass condensed into stars that is transferred back to the remaining gas, estimating the feedback efficiency, of $\epsilon = 3.9 \times 10^{-5}$, and 10% of the total pressure due to a non-thermal component. This solution agrees with hydrodynamic simulations and can reproduce some observations from X-ray scaling relations, which speaks to the validity of the OBB Model.

4.2. *GNFW Models*

To normalize the density and pressure profiles, two generalized Navarro–Frenk–White profiles (GNFW) are used. The first originates from the standard NFW model, based on density:

$$\rho_{\rm GNFW}(x) = \rho_0 (x/x_{c,k})^{\gamma_k} [1 + (x/x_{c,k})^{\alpha_k}]^{-\frac{\beta_k - \gamma_k}{\alpha_k}},$$

$$\rho_{\rm gas}(x) = \rho_{\rm GNFW}(x)\, \rho_{\rm cr}(z)\, f_b,$$

where $x \equiv r/R_{200}$, $x_{c,k}$ is a core scale, $(\alpha_k, \beta_k, \gamma_k)$ are the slopes at $x \sim 1$, $x \gg 1$, and $x \ll 1$, respectively. $\rho_{\rm cr}(z)$ is the critical density of the Universe at redshift z, and $f_b = \Omega_b/\Omega_m$ is the baryon fraction. This model is subject to degeneracy as the parameters that are sensitive to profiles at small radii are not constrained well. Thus, two parameters are fixed in this model: $\gamma_k = -0.2$ and $\alpha_k = 1$.

A slightly modified GNFW profile is used to model the thermal pressure profile:

$$P_{\rm GNFW}(x) = P_0 (x/x_{c,t})^{\gamma_t} [1 + (x/x_{c,t})^{\alpha_t}]^{-\beta_t},$$

$$P_{\rm th}(x) = P_{\rm GNFW}(x) P_{200},$$

where $P_{200} = G M_{200}\, 200\, \rho_{\rm cr}(z)\, f_b/(2R_{200})$, $x_{c,t}$ is a core scale, and $(\alpha_t, \beta_t, \gamma_t)$ are the slopes at $x \sim 1$, $x \gg 1$, and $x \ll 1$, respectively. This profile is subject to the same degeneracies at smaller radii, therefore two parameters are fixed: $\gamma_t = -0.3$ and

$$x_{c,t} = 0.497 \times (M_{200}/10^{14} M_\odot)^{-0.00865} \times (1+z)^{0.731}.$$

4.3. *Results of Feedback Model*

Using the models described above, Battaglia et al were able to effectively model tSZ and kSZ effects with feedback present. Below is a comparison of both profiles with observational data from the Atacama Cosmological Telescope, denoted by ACT f150. The kSZ profile shows a comparison between the current study and NFW profiles, while the tSZ plot includes corrections from dust.

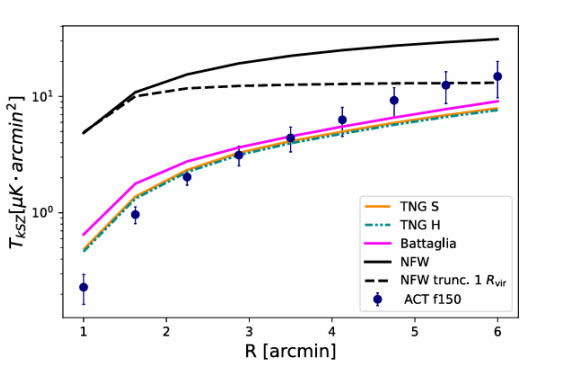

Figure 5. kSZ Effect vs. Radius S. Amodeo et al. (2021)

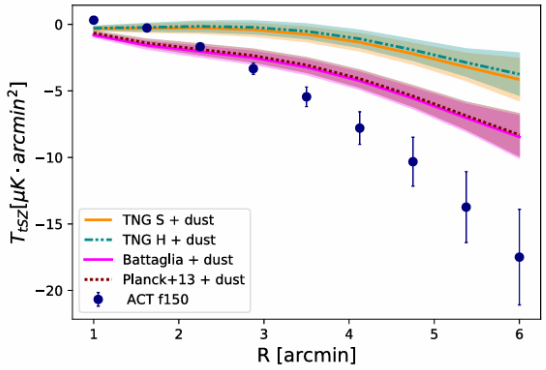

Figure 6. tSZ Effect vs. Radius S. Amodeo et al. (2021)

The kSZ curve improved considerably on the NFW profiles in comparison to observable data, while it only deviates slightly from the Illustris/TNG profiles. In comparison, the tSZ curve matches the observable data significantly closer than the Illustris/TNG profiles. However, there is still a notable deviation in data from larger radii.

In combining kSZ and tSZ measurements, the thermal energy injected to the gas from AGN and supernovae is found to be injected into the gas from AGN and supernovae, $\epsilon = (40 \pm 9) \times 10^{-6}$ (1σ), with a 23% relative uncertainty. From this result it is estimated that the energy injected by feedback is 30% of the total binding energy of the system. Furthermore, the upper limit for the amplitude of the non-thermal pressure profile is found as $\alpha_{\rm Nth} < 0.2$ (2σ). This implies that less than 20% of the total electron pressure within R_{200} is due to a non-thermal component.

Two important conclusions can be drawn from this study: including a baryon correction reduces but does not fully reconcile the difference with galaxy-galaxy lensing measurement, and the current feedback model underestimates CGM pressure. Battaglia's study demonstrates the power of joint tSZ and kSZ cross-correlation measurements in studying the distribution of baryons in the CGM of CMASS galaxy groups. This power can be used to eventually piece together galaxy assembly information in the presence of unknown baryon profiles and can reveal important information about feedback processes. These discrepancies could possibly be explained by the lack of distinction between ejective and preventive feedback. In attributing all feedback to the AGN, we fail to recognize the feedback due to accretion shock in galaxy formation.

5. THE SUNYAEV ZEL'DOVICH EFFECT ON CGM AND ICM

Since the genesis of the 'missing baryon problem', it has been theorized that much of the missing baryonic matter resides in both the circumgalactic medium (CGM) and intracluster medium (ICM). While traditional X-ray observations trace only the densest, hottest regions of clusters, the Sunyaev Zel'dovich effect (SZE) allows for the detection of more diffuse gas, allowing us to understand how baryonic matter is distributed in filaments, clusters, etc.

As mentioned previously, the thermal Sunyaev-Zeldovich effect (tSZ) measures the integrated electron pressure along the line of sight, which is proportional to the thermal pressure. Thus, the tSZ signal is sensitive to hot, ionized gas regions present in both the CGM and ICM. The pressure maps that arise from the tSZ are particularly important in modeling feedback from AGN and supernovae, as seen in the previous section. Alternatively, the kinetic Sunyaev–Zel'dovich effect (kSZ) is sensitive to the bulk motions of free electrons along the line of sight. As the kSZ depends on the peculiar velocity of electrons, it is proportional to the density profile of a given region. Thus, the kSZ enables the study of baryons over sparse, large regions, both present in the CGM and ICM.

In combining both tSZ and kSZ measurements, it becomes possible to separately constrain these pressure and density profiles. In terms of the ICM, this allows us to study energy injection– not just from AGN and supernovae, but also from galactic winds, merger shocks, and cosmic ray pressure. Similarly to the ICM, the CGM can be studied using the SZE in regards to finding out which feedback mechanisms are responsible for the behavior of a given region. In essence, kSZ can be used to reveal the underlying gas reservoir even if it is cold (on the order of 10 K). This gives us our 'fuel' for star formation, as if not for other physical processes inherent within galaxy formation, $M_{\rm gas}$ is the only parameter responsi-

ble for star formation. Combining this with tSZ, which can highlight the regions affected by feedback, we can tell an accurate story of what is happening in the ICM and CGM. This gives us insight into galaxy formation and evolution that is not possible through traditional observation techniques.

In conclusion, the Sunyaev–Zel'dovich Effect, through its two manifestations, provides a view of the thermodynamic and kinematic state of gas in cosmic structures, particularly the CGM and ICM. As observational sensitivity continues to improve with facilities like ACT, SPT, and future experiments, the SZE will play an increasingly vital role in piecing together the complexities of galaxy formation.

APPENDIX

A. LIST OF VARIABLES

- λ — original photon wavelength
- λ' — scattered photon wavelength
- h — Planck's constant
- m_e — electron rest mass
- c — speed of light
- θ — scattering angle of the photon
- ν — observing frequency
- $x = \frac{h\nu}{k_B T_{\rm CMB}}$ — dimensionless frequency parameter
- $f(\nu) = x\coth(x/2) - 4$ — frequency-dependent spectral distortion function
- $\Delta T_{\rm tSZ}$ — temperature shift in the CMB from the thermal SZ effect
- $\Delta T_{\rm kSZ}$ — temperature shift in the CMB from the kinetic SZ effect
- $T_{\rm CMB}$ — mean temperature of the cosmic microwave background
- y — Compton-y parameter (line-of-sight integral of electron pressure)
- $y(\theta)$ — y-parameter as a function of angular position θ
- σ_T — Thomson scattering cross-section
- $\int_{\rm los}$ — integration along the line of sight
- $P_e(r)$ — electron pressure profile at 3D radius r
- l — line-of-sight coordinate
- $r = \sqrt{l^2 + d_A(z)^2|\theta|^2}$ — 3D radius in spherical coordinates
- $d_A(z)$ — angular diameter distance to redshift z
- n_e — electron number density
- v_p — peculiar velocity of electrons
- τ — optical depth due to Thomson scattering
- $\tau_{\rm gal}$ — galaxy optical depth

- v_r — line-of-sight peculiar velocity (RMS value)
- B_x, B_y — projected baseline components for interferometry
- $u = \frac{B_x}{\lambda},\ v = \frac{B_y}{\lambda}$ — spatial frequencies in interferometric observations
- $I(l, m)$ — sky brightness distribution as a function of angular coordinates
- $V(u, v)$ — complex visibility (Fourier transform of $I(l, m)$)
- $\rho_{\mathrm{DM}}(x)$ — dark matter density profile (NFW)
- $x = r/r_s$ — scaled radius in NFW profile
- c_{NFW} — concentration parameter
- $\rho_{\mathrm{gas}}(r)$ — gas density profile
- $P_{\mathrm{tot}}(r)$ — total gas pressure profile
- Γ — polytropic index
- $\theta(r)$ — polytropic variable
- $\Phi(r)$ — gravitational potential
- ϵ — feedback efficiency
- M_* — stellar mass
- ΔE_p — energy from boundary expansion/contraction
- α_{Nth} — non-thermal pressure fraction
- $\rho_{\mathrm{GNFW}}(x)$ — generalized NFW density profile
- $P_{\mathrm{GNFW}}(x)$ — generalized NFW pressure profile
- $\rho_c(z)$ — critical density of the universe at redshift z
- f_b — baryon fraction, $f_b = \Omega_b/\Omega_m$
- P_{200} — characteristic pressure scale at R_{200}
- R_{200} — radius within which the mean density is 200 times the critical density

REFERENCES

Amodeo, S., Battaglia, N., Schaan, E., et al. 2021, Physical Review D, 103, 063514, doi: 10.1103/PhysRevD.103.063514

Carlstrom, J. E., Holder, G. P., & Reese, E. D. 2002, Annual Review of Astronomy and Astrophysics, 40, 643, doi: 10.1146/annurev.astro.40.060401.093803

Schaan, E., Ferraro, S., Amodeo, S., et al. 2021, Physical Review D, 103, 063513, doi: 10.1103/PhysRevD.103.063513

Sunyaev, R. A., & Zel'dovich, Y. B. 1972, Comments on Astrophysics and Space Physics, 4, 173

Sunyaev, R. A., & Zel'dovich, Y. B. 1980, Annual Review of Astronomy and Astrophysics, 18, 537, doi: 10.1146/annurev.aa.18.090180.002541